neuron pairs and astrocytes that exhibited calcium activity at the same time as the neuronal synchronization (Fig. 4*D*). The neuron–glia distances were significantly smaller than those obtained from their surrogate datasets ($P < 0.05$, Kolmogorov–Smirnov test), suggesting a non-random spatial arrangement in glia-related neuronal synchronization. However, the average distance was 95 ± 8 μm ($n = 3834$ pairs), which is larger than the size of a single astrocyte territory (Bushong *et al.* 2002). This indicates that not all correlated activity is explained by the inter-soma distance alone. The lack of an apparent proximity in neuronal and glial activity may be attributable to the complexity of dendritic morphology. To test this idea, two CA3 pyramidal cells within an imaging region

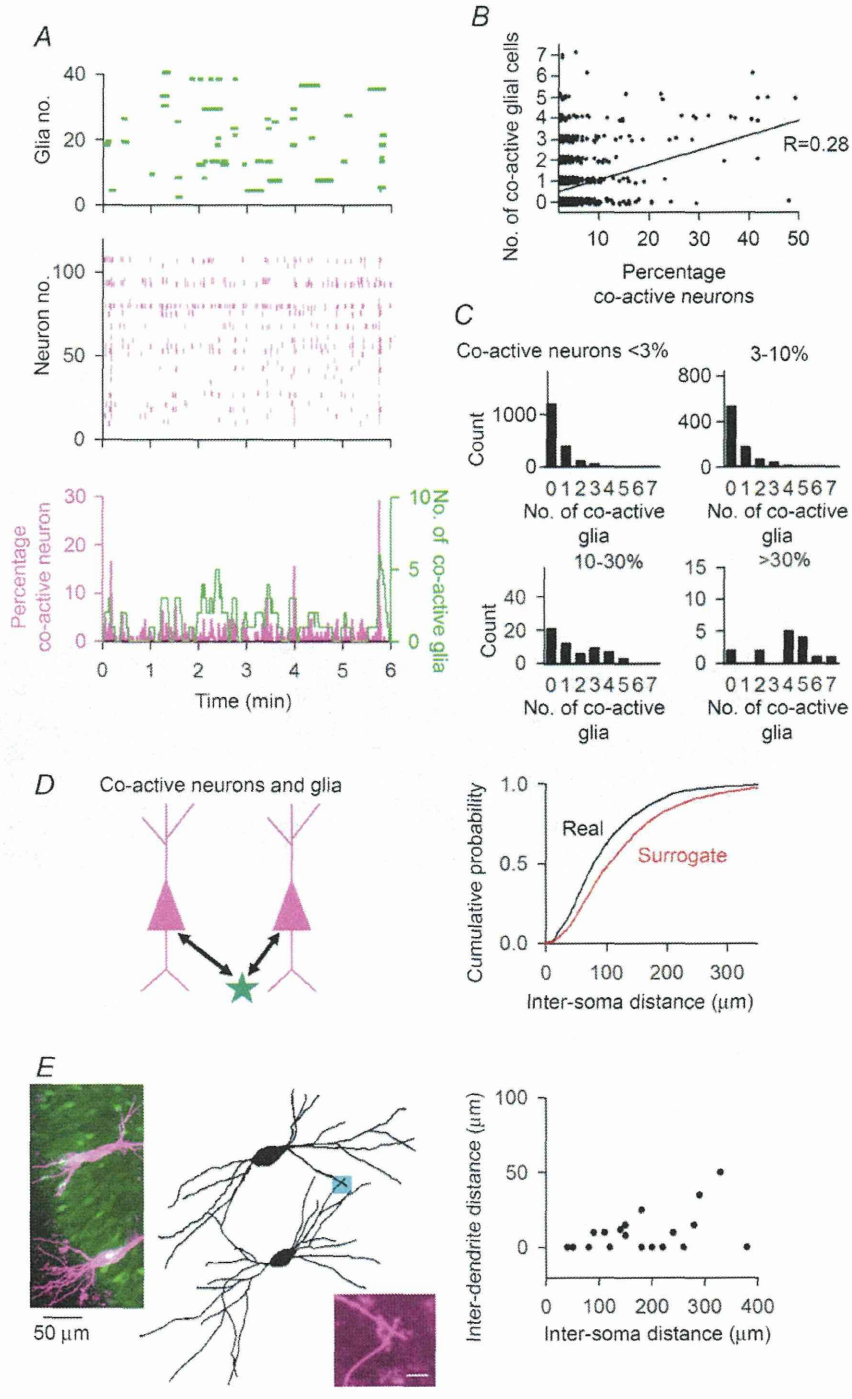

Figure 4. Correlated activity of neuronal and glial networks
A, calcium activity of astrocytes (*top*) and neurons (*middle*). The bottom time histogram represents the percentage of co-active neurons and the number of co-active glial cells. *B*, the number of co-active glial cells plotted against the percentage of co-active neurons ($R = 0.28$, $P < 0.01$, $n = 2741$). *C*, distribution of the number of co-active glial cells at the period when the percentage of co-active neurons is <3% ($n = 1825$), 3–10% ($n = 843$), 10–30% ($n = 58$) and >30% ($n = 15$). The data were reconstructed from the plot in *B*. *D*, cumulative distribution of soma-to-soma distances between co-active neurons and glial cells. Surrogate datasets were created by randomly selecting glial cells in the same imaging field. $P < 0.01$, Kolmogorov–Smirnov test. *E*, (*left*) representative image of Alexa 594-injected neurons after whole-cell recordings superimposed on OGB-1-loaded cells. In this example, the inter-soma distance is 168 μm, and the minimum inter-dendrite distance is 0 μm. The point represents a contact site, which is magnified in the right bottom inset. Scale bar = 5 μm. (*Right*) In each neuron pair, the minimum inter-dendrite distance was plotted as a function of the inter-soma distance ($n = 19$ neuron pairs).

(400 × 400 μm) were randomly selected and labelled by Alexa Fluor 594 through whole-cell patch-clamp pipettes (Fig. 4*E*). In 9 of 19 neuron pairs, a part of the dendrites from two neurons overlapped with each other (i.e. minimum inter-dendrite distance = 0 μm). In 18 of 19 pairs, the minimum inter-dendrite distance was less than 50 μm (Fig. 4*E*, right). The spatial apposition suggests that, within the range of our imaging field, nearly all neuron pairs can be linked to a single astrocyte territory through their processes.

Astrocytes modulate the temporal dynamics of the neuronal population

To directly investigate whether glial cells regulate the formation of patterned activity in neuronal circuits, the calcium signal of astrocytes was hampered by an intracellular infusion of BAPTA, a calcium chelator that can buffer intracellular calcium ions (Serrano *et al.* 2006; Navarrete & Araque, 2010; Di Castro *et al.* 2011; Panatier *et al.* 2011; Poskanzer & Yuste, 2011). To inject BAPTA into multiple astrocytes, we used a single-cell electroporation technique (Judkewitz *et al.* 2009; Ohkura *et al.* 2012). Compared with the loading of chemical compounds through whole-cell pipettes, single-cell electroporation has the advantage of being able to sequentially introduce compounds into multiple cells within a short time. Indeed, we were able to load BAPTA into 20 adjacent cells one by one within 5 min. The BAPTA loading was confirmed by co-loading with Alexa 594-dextran (Fig. 5*A*). The fluorescent signals did not leak into neighbouring neuropils, demonstrating the selective loading of BAPTA into astrocyte compartments. Unlike Alexa 594-dextran, BAPTA freely spreads to neighbouring astrocytes through gap junctions; thus, virtually all astrocytes in an imaged area were expected to be loaded with BAPTA. Consistent with this, the spontaneous calcium events of those astrocytes, including the indirectly loaded cells, were almost completely abolished after the multicellular BAPTA dialysis (Fig. 5*A*, right).

First, we examined the effect of BAPTA dialysis on nearby synaptic transmission. We obtained simultaneous whole-cell recordings from synaptically connected pairs of CA3 pyramidal cells (Fig. 5*B*). The presynaptic neurons were injected with a brief depolarizing current 50–100 times every 10 s to evoke single action potentials, and unitary postsynaptic currents were monitored from the postsynaptic cells that were clamped at a voltage of −70 mV. After recordings of the basal unitary postsynaptic currents for 5 min, BAPTA was loaded into 5–12 astrocytes located around the postsynaptic dendrites. Similar to previous studies using minimal stimulation of dentate gyrus synapses (Di Castro *et al.* 2011) and CA1 synapses (Panatier *et al.* 2011) in acute hippocampus slices, the astrocytic BAPTA significantly reduced the amplitude of

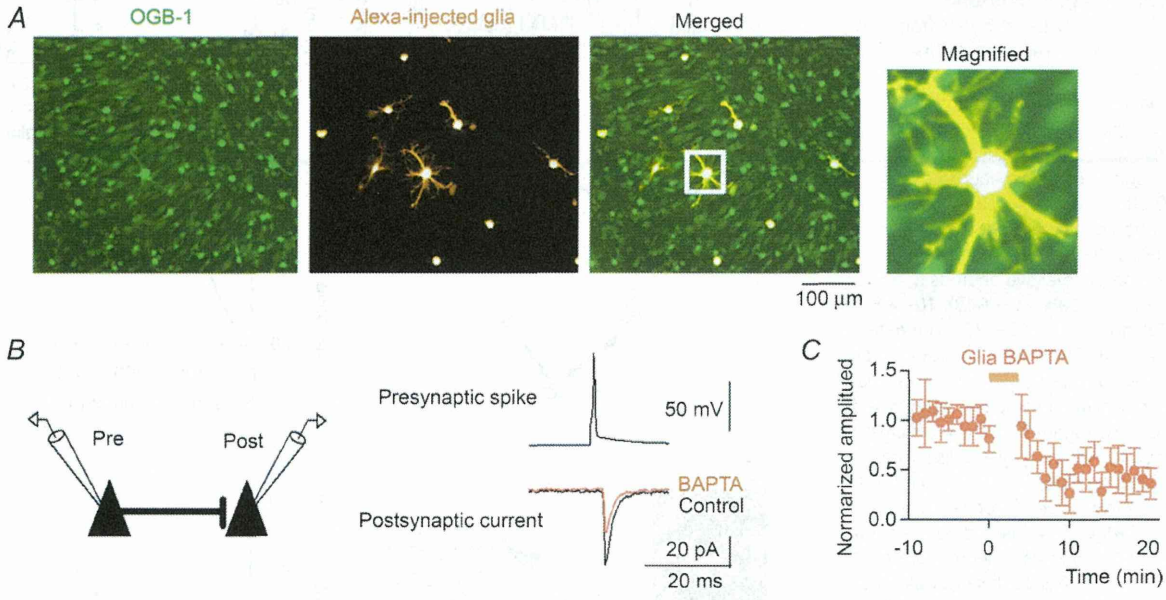

Figure 5. Calcium chelation in astrocytes attenuates nearby synaptic transmission
A, OGB-1-loaded CA3 cells and astrocytes co-loaded with BAPTA and Alexa 594-dextran were confocally imaged and merged in the right panel. The region in the white square is magnified in the right inset. *B*, dual whole-cell recordings were obtained from a synaptically coupled pair of CA3 pyramidal cells. Averaged unitary postsynaptic currents triggered by single presynaptic spikes were recorded before and after intracellular BAPTA injection. *C*, the amplitudes of the postsynaptic currents were normalized to the baseline level before BAPTA infusion and plotted as a function of time relative to the BAPTA injection (n = 4 cells). Error bars are SEM.

the unitary postsynaptic currents in CA3 pyramidal cells by 49.3 ± 22.2% (Fig. 5*C*; $P = 0.0031$, $t_4 = 6.36$, paired-t test, $n = 5$ cells).

Next, we investigated whether the blockade of astrocyte calcium signals affects the collective behaviour of neuronal populations. Figure 6*A* depicts representative rastergrams of neuronal and astrocyte calcium events in a slice in which astrocytes were electroporated with or without BAPTA by our electroporation method. There were no significant differences between the BAPTA-free slices (EP Without BAPTA, $n = 6$ slices) and the BAPTA-treated slices (EP With BAPTA, $n = 6$ slices) in the percentage of

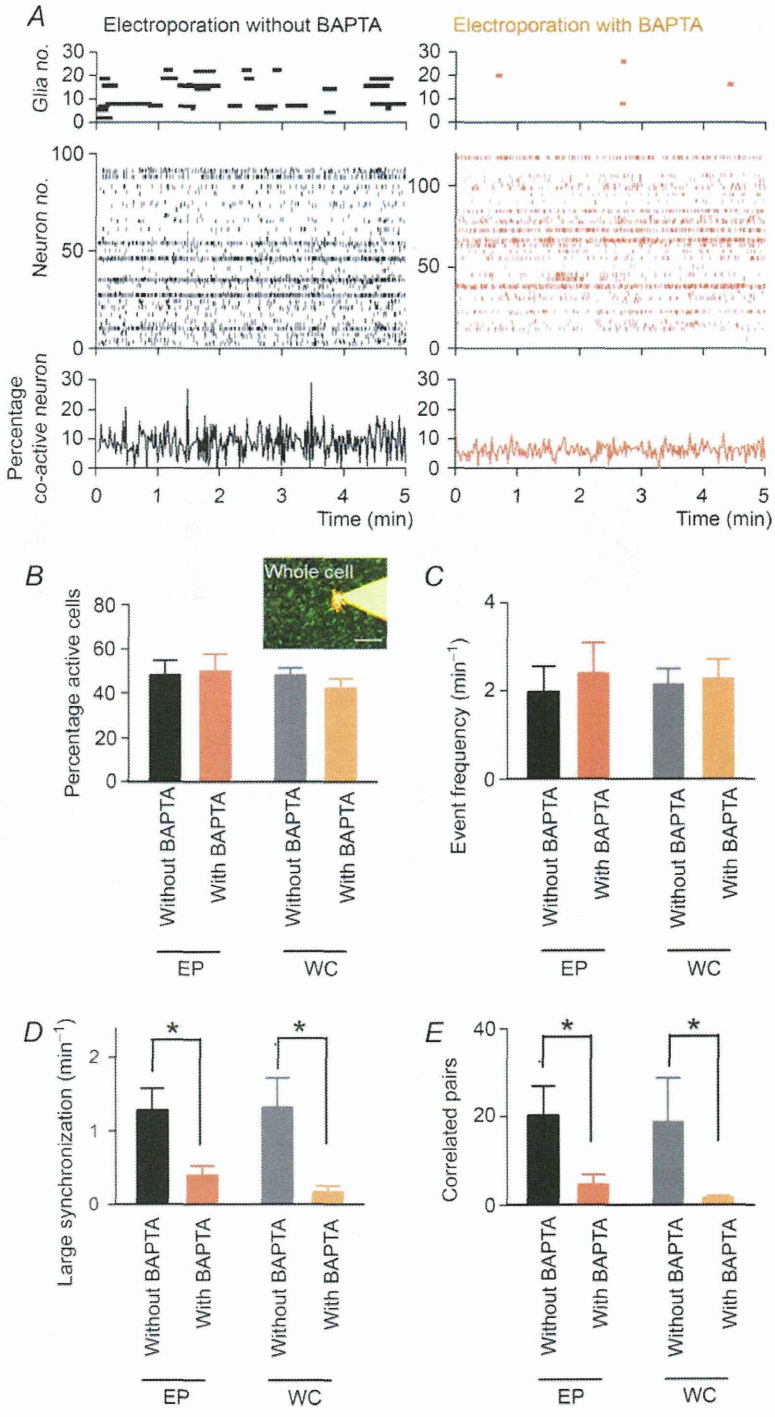

Figure 6. Calcium chelation in astrocytes attenuates neuronal synchronization
A, the calcium activity of astrocytes (*top*) and neurons (*middle*) is compared between slices in which 20 astrocytes were electroporated with BAPTA (*right*) or no BAPTA (*left*). The bottom time histograms represent the percentage of co-active neurons (100 ms bin). *B* and *C*, the percentage of active neurons in a given 5 min time period (*B*) and the mean frequency of neuronal events (*C*). BAPTA was injected by electroporation of astrocyte populations (EP) or whole-cell patching of a single astrocyte (WC, *inset*). EP Without BAPTA, $n = 6$ slices; EP With BAPTA, $n = 6$ slices; WC Without BAPTA, $n = 5$ slices; WC With BAPTA, $n = 5$ slices. Scale bar = 50 μm. *D* and *E*, the frequency of large synchronization (*D*) and the number of highly correlated neuron pairs (*E*). Error bars are SEM, $^*P < 0.05$, Student's t test.

active neurons (Fig. 6*B*; $P = 0.47$, $t_{10} = 0.75$, Student's t test), the mean frequency of neuronal events (Fig. 6*C*; $P = 0.69$, $t_{10} = 0.41$, Student's t test) or the distribution of neuronal event frequencies ($P = 0.10$, $D_{576} = 0.10$, Kolmogorov–Smirnov test). Therefore, the treatment of astrocytes with BAPTA was unlikely to influence the level of spontaneous neuronal activity *per se*. Nonetheless, we found that BAPTA treatment interfered with neuronal synchronization; in the BAPTA-treated slices, both the frequency of large synchronization (Fig. 6*D*; $P = 0.012$, $t_{10} = 3.02$, Student's t test) and the number of highly correlated pairs (Fig. 6*E*; $P = 0.017$, $t_{10} = 2.83$, Student's t test) were significantly lower than those in the BAPTA-free slices. We also performed intracellular BAPTA dialysis of a single astrocyte using whole-cell recording with a pipette solution containing 10 mM BAPTA (Panatier *et al.* 2011). Consistent with the results from the above electroporation method, the BAPTA injection into an astrocyte through a whole-cell pipette (WC With BAPTA) significantly reduced the frequency of large synchronization (Fig. 6*D*; $P = 0.013$, $t_8 = 3.19$, Student's t test) and the number of highly correlated pairs (Fig. 6*E*; $P = 0.019$, $t_8 = 2.92$, Student's t test) compared with those in the BAPTA-free condition (WC Without BAPTA). These results suggest that astrocyte calcium signalling is necessary for sustaining the temporally organized dynamics of a neuronal population.

To investigate the mechanisms underlying glia-related neuronal synchrony, we examined the pharmacological actions of glutamatergic and purinergic antagonists. Among the tested inhibitors, PPADS, a P2 ATP receptor antagonist, and MCPG, a group I and II metabotropic glutamate receptor (mGluR) antagonist, tended to affect neuronal dynamics. In the presence of PPADS, both the frequency of large synchronization and the number of correlated neuronal pairs were partially reduced, whereas the total neuronal firing rates remained unchanged (Fig. 7*A*). An MCPG application reduced the frequency of large neuronal synchronization (Fig. 7*B*, middle) without altering the number of correlated cell pairs (Fig. 7*B*, bottom). No differences in these parameters were found in the presence of AP5, an *N*-methyl-D-aspartate (NMDA)

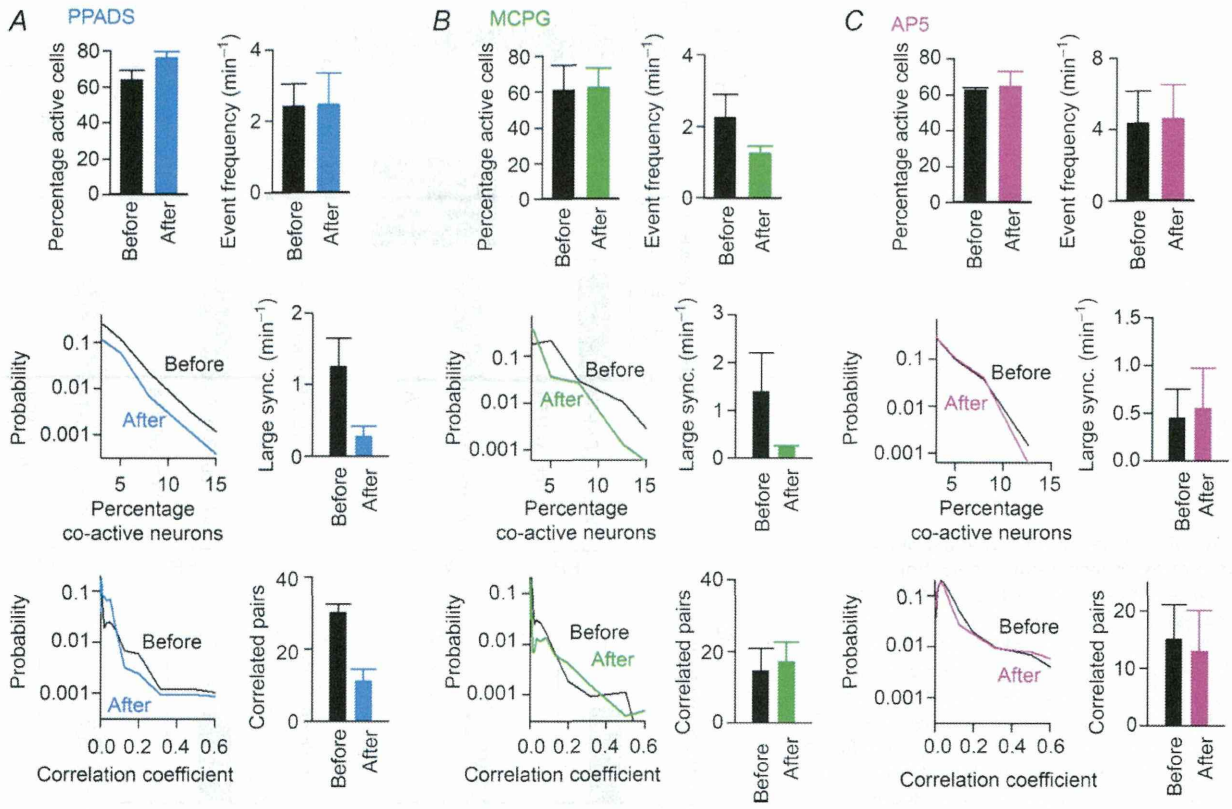

Figure 7. Pharmacological inhibition of synchronized neuronal activity
A, (*top*) the percentage of active neurons in a given 5 min time period and the average frequency of neuronal events before and after bath application of PPADS ($n = 4$ slices). (*middle*) Distribution of the percentage of co-active cells (*left*) and the frequency of large synchronization (*right*), which were calculated as described in Fig. 3C. (*bottom*) Distribution of correlation values between neuron pairs (*left*) and the number of highly correlated pairs (*right*), which were calculated as described in Fig. 3*D*. *B*, same as in *A* but for MCPG application ($n = 4$ slices). *C*, same as in *A* but for AP5 application ($n = 4$ slices). Error bars are SEM.

receptor antagonist (Fig. 7*C*), indicating that activation of NMDA receptors is not involved in the synchronized patterns of neurons.

Finally, we examined whether the astrocyte calcium elevations were sufficient to increase neuronal synchronization. Eight to 12 astrocytes were electroporated with NP-EGTA, a UV-sensitive caged calcium reagent, and these astrocytes were illuminated with UV light (330 nm) with a diameter of 150 μm for 5–10 s. To prevent excessive neuronal activation after uncaging, the baseline activity level was lowered by aCSF that consisted of 3.0 mM K^+, 1.8 mM Ca^{2+} and 1.8 mM Mg^{2+}. The UV-induced uncaging significantly increased the frequency of large synchronization (Fig. 8*B*; $P = 0.0021$, $t_4 = 7.11$, paired t test) and the number of highly correlated pairs (Fig. 8*C*; $P = 0.009$, $t_4 = 4.76$, paired t test). Similar results were obtained when the caged compound was intracellularly dialysed into a single astrocyte by a whole-cell pipette (large synchronization, $P = 0.0061$, $t_3 = 6.97$; number of highly correlated pairs, $P = 0.027$, $t_3 = 4.03$).

Discussion

Previous studies of neuron–astrocyte communication have shown the role of astrocyte calcium signals in regulating the basal activity of a small number of synapses (Di Castro *et al.* 2011; Panatier *et al.* 2011). In the condition in which calcium signals are buffered in astrocyte populations, we showed that synchronized neuronal activity is prominently reduced, which supports the proposal that astrocytes can maintain basal neuronal function at the network level.

Note, however, that our study was performed using young slice preparations. The mechanisms of astrocyte calcium signalling differ between the adult brain and the young brain (Sun *et al.* 2013) or between slices and *in vivo* measurements (Takano *et al.* 2014). In addition, organotypic slice cultures undergo re-extension of astrocyte processes, as shown in Fig. 1, and substantial remodelling of synaptic connections. To extrapolate our results to a higher order of brain functions, further studies will be needed with other types of experimental preparations using advanced technical approaches.

The BAPTA treatment reduced, but did not completely abolish, the basal synaptic transmission. Likewise, it weakened, but did not completely block, the neuronal synchronization. Therefore, astrocytes are not indispensable to synaptic transmission or synchronization, but they are probably involved in neuromodulation through gliotransmitters. From a series of tested pharmacological inhibitors, we found that P2 receptor blockade showed effects that were most similar to calcium buffering in astrocytes (i.e. both the frequency of large synchronization and the number of correlated neuronal pairs were decreased without altering the total neuronal firing rates). These results imply that P2 receptor activation might be responsible for the glial maintenance of neuronal synchronization. However, bath application of drugs is not cell-type specific; thus, we cannot exclude the possibility that these pharmacological actions were simply due to the inhibition of neuronal receptors that are independent of glia-related

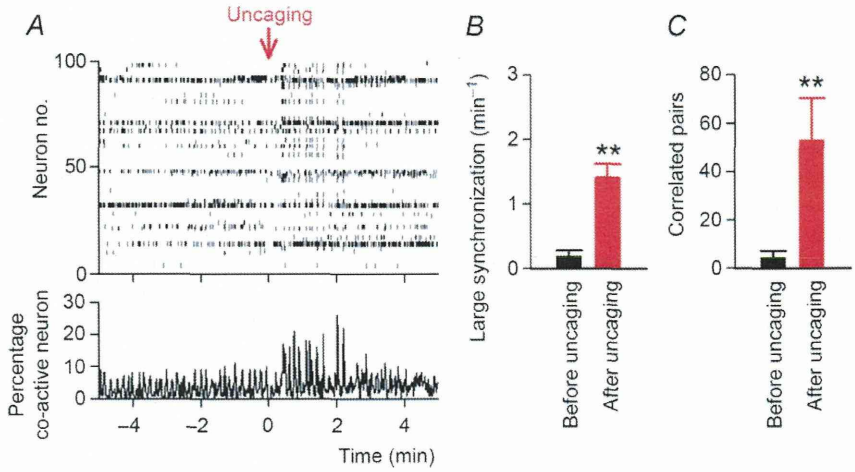

Figure 8. Calcium uncaging in astrocytes facilitates neuronal synchronization
A, NP-EGTA-loaded astrocytes were illuminated with UV for 5 s at time 0 min (Uncaging) while calcium activity was monitored in the surrounding neurons. The recording was performed in aCSF containing 3.0 mM K^+, 1.8 mM Ca^{2+} and 1.8 mM Mg^{2+}. *B* and *C*, the frequencies of large synchronization (*B*) and the number of highly correlated pairs (*C*) were compared between the control period before uncaging and the 2 min period after uncaging; $n = 3299$ pairs between 531 cells from five slices. Error bars are SEM, $^{**}P < 0.01$, paired t test.

pathways. Application of MCPG, an mGluR antagonist, abolished large neuronal synchronization, but these effects could be simply explained by a decrease in the overall frequency of neuronal calcium events (Fig. 7*B*, top), which makes it difficult to determine whether metabotropic glutamate receptors are involved in glia-induced neuronal synchronization. Another possible mechanism is the breakdown of glial–neuronal metabolic interactions. Disruption of the intracellular ion equilibrium by calcium buffering in astrocytes may cause a reduction in the delivery of metabolic substrates to neurons, leading to the dysfunction of organized neuronal networks (Belanger *et al.* 2011). To isolate the effect of astrocytes and determine the detailed mechanisms of complex network dynamics, further investigation is required using molecular and genetic tools to selectively manipulate targeted molecules in a cell type-specific manner.

Assuming that organized temporal patterns of neurons contribute to information processing and memory storage in the brain (Zohary *et al.* 1994; Vaadia *et al.* 1995; deCharms & Merzenich, 1996; Riehle *et al.* 1997; Steinmetz *et al.* 2000), astrocyte calcium signal may play a pivotal role in fundamental brain function by sustaining functional clusters of neurons.

References

Allen NJ & Barres BA (2009). Neuroscience: Glia – more than just brain glue. *Nature* **457**, 675–677.

Belanger M, Allaman I & Magistretti PJ (2011). Brain energy metabolism: focus on astrocyte–neuron metabolic cooperation. *Cell Metab* **14**, 724–738.

Bernardinelli Y, Salmon C, Jones EV, Farmer WT, Stellwagen D & Murai KK (2011). Astrocytes display complex and localized calcium responses to single-neuron stimulation in the hippocampus. *J Neurosci* **31**, 8905–8919.

Bushong EA, Martone ME, Jones YZ & Ellisman MH (2002). Protoplasmic astrocytes in CA1 stratum radiatum occupy separate anatomical domains. *J Neurosci* **22**, 183–192.

deCharms RC & Merzenich MM (1996). Primary cortical representation of sounds by the coordination of action-potential timing. *Nature* **381**, 610–613.

Di Castro MA, Chuquet J, Liaudet N, Bhaukaurally K, Santello M, Bouvier D, Tiret P & Volterra A (2011). Local Ca^{2+} detection and modulation of synaptic release by astrocytes. *Nat Neurosci* **14**, 1276–1284.

Gordon GR, Iremonger KJ, Kantevari S, Ellis-Davies GC, MacVicar BA & Bains JS (2009). Astrocyte-mediated distributed plasticity at hypothalamic glutamate synapses. *Neuron* **64**, 391–403.

Halassa MM & Haydon PG (2010). Integrated brain circuits: astrocytic networks modulate neuronal activity and behaviour. *Annu Rev Physiol* **72**, 335–355.

Henneberger C, Papouin T, Oliet SH & Rusakov DA (2010). Long-term potentiation depends on release of D-serine from astrocytes. *Nature* **463**, 232–236.

Judkewitz B, Rizzi M, Kitamura K & Hausser M (2009). Targeted single-cell electroporation of mammalian neurons *in vivo*. *Nat Protoc* **4**, 862–869.

Koyama R, Muramatsu R, Sasaki T, Kimura R, Ueyama C, Tamura M, Tamura N, Ichikawa J, Takahashi N, Usami A, Yamada MK, Matsuki N & Ikegaya Y (2007). A low-cost method for brain slice cultures. *J Pharmacol Sci* **104**, 191–194.

Kuga N, Sasaki T, Takahara Y, Matsuki N & Ikegaya Y (2011). Large-scale calcium waves traveling through astrocytic networks *in vivo*. *J Neurosci* **31**, 2607–2614.

Min R & Nevian T (2012). Astrocyte signalling controls spike timing-dependent depression at neocortical synapses. *Nat Neurosci* **15**, 746–753.

Navarrete M & Araque A (2010). Endocannabinoids potentiate synaptic transmission through stimulation of astrocytes. *Neuron* **68**, 113–126.

Nimmerjahn A, Mukamel EA & Schnitzer MJ (2009). Motor behaviour activates Bergmann glial networks. *Neuron* **62**, 400–412.

Ohkura M, Sasaki T, Kobayashi C, Ikegaya Y & Nakai J (2012). An improved genetically encoded red fluorescent Ca^{2+} indicator for detecting optically evoked action potentials. *PLoS One* **7**, e39933.

Panatier A, Vallee J, Haber M, Murai KK, Lacaille JC & Robitaille R (2011). Astrocytes are endogenous regulators of basal transmission at central synapses. *Cell* **146**, 785–798.

Perea G & Araque A (2005). Properties of synaptically evoked astrocyte calcium signal reveal synaptic information processing by astrocytes. *J Neurosci* **25**, 2192–2203.

Poskanzer KE & Yuste R (2011). Astrocytic regulation of cortical UP states. *Proc Natl Acad Sci U S A* **108**, 18453–18458.

Riehle A, Grun S, Diesmann M & Aertsen A (1997). Spike synchronization and rate modulation differentially involved in motor cortical function. *Science* **278**, 1950–1953.

Sasaki T, Kuga N, Namiki S, Matsuki N & Ikegaya Y (2011). Locally synchronized astrocytes. *Cereb Cortex* **21**, 1889–1900.

Sasaki T, Matsuki N & Ikegaya Y (2007). Metastability of active CA3 networks. *J Neurosci* **27**, 517–528.

Sasaki T, Takahashi N, Matsuki N & Ikegaya Y (2008). Fast and accurate detection of action potentials from somatic calcium fluctuations. *J Neurophysiol* **100**, 1668–1676.

Schummers J, Yu H & Sur M (2008). Tuned responses of astrocytes and their influence on hemodynamic signals in the visual cortex. *Science* **320**, 1638–1643.

Serrano A, Haddjeri N, Lacaille JC & Robitaille R (2006). GABAergic network activation of glial cells underlies hippocampal heterosynaptic depression. *J Neurosci* **26**, 5370–5382.

Steinmetz PN, Roy A, Fitzgerald PJ, Hsiao SS, Johnson KO & Niebur E (2000). Attention modulates synchronized neuronal firing in primate somatosensory cortex. *Nature* **404**, 187–190.

Sun W, McConnell E, Pare JF, Xu Q, Chen M, Peng W, Lovatt D, Han X, Smith Y & Nedergaard M (2013). Glutamate-dependent neuroglial calcium signalling differs between young and adult brain. *Science* **339**, 197–200.

Takahashi N, Sasaki T, Matsumoto W, Matsuki N & Ikegaya Y (2010). Circuit topology for synchronizing neurons in spontaneously active networks. *Proc Natl Acad Sci U S A* **107**, 10244–10249.

Takano T, He W, Han X, Wang F, Xu Q, Wang X, Oberheim Bush NA, Cruz N, Dienel GA & Nedergaard M (2014). Rapid manifestation of reactive astrogliosis in acute hippocampal brain slices. *Glia* **62**, 78–95.

Takata N, Mishima T, Hisatsune C, Nagai T, Ebisui E, Mikoshiba K & Hirase H (2011). Astrocyte calcium signalling transforms cholinergic modulation to cortical plasticity *in vivo*. *J Neurosci* **31**, 18155–18165.

Vaadia E, Haalman I, Abeles M, Bergman H, Prut Y, Slovin H & Aertsen A (1995). Dynamics of neuronal interactions in monkey cortex in relation to behavioural events. *Nature* **373**, 515–518.

Wang X, Lou N, Xu Q, Tian GF, Peng WG, Han X, Kang J, Takano T & Nedergaard M (2006). Astrocytic Ca^{2+} signalling evoked by sensory stimulation *in vivo*. *Nat Neurosci* **9**, 816–823.

Wittner L, Henze DA, Zaborszky L & Buzsaki G (2007). Three-dimensional reconstruction of the axon arbor of a CA3 pyramidal cell recorded and filled *in vivo*. *Brain Struct Funct* **212**, 75–83.

Zohary E, Shadlen MN & Newsome WT (1994). Correlated neuronal discharge rate and its implications for psychophysical performance. *Nature* **370**, 140–143.

Additional information

Competing interests

None declared.

Author contributions

T.S. designed the research; T.S. collected and analysed the slice imaging and patch-clamp recording data while T.I. performed pharmacological experiments. R.N. performed the immunohistochemical investigation. R.A. and A.A. performed the *in vivo* imaging. M.N. and Y.I. supervised the project. T.S. and Y.I. wrote the manuscript. All authors read and approved the final submission. The research was conducted at The University of Tokyo.

Funding

This work was partly supported by Grants-in-Aid for Science Research on Innovative Areas, 'Mesoscopic Neurocircuitry' (No. 22115003), from the Ministry of Education, Culture, Sports, Science and Technology of Japan and by the Funding Program for Next Generation World-Leading Researchers (LS023).

Systems/Circuits

Operant Conditioning of Synaptic and Spiking Activity Patterns in Single Hippocampal Neurons

Daisuke Ishikawa,[1] Nobuyoshi Matsumoto,[1] Tetsuya Sakaguchi,[1] Norio Matsuki,[1] and Yuji Ikegaya[1,2]

[1]Laboratory of Chemical Pharmacology, Graduate School of Pharmaceutical Sciences, University of Tokyo, Tokyo 113-0033, Japan, and [2]Center for Information and Neural Networks, Suita City, Osaka 565-0871, Japan

Learning is a process of plastic adaptation through which a neural circuit generates a more preferable outcome; however, at a microscopic level, little is known about how synaptic activity is patterned into a desired configuration. Here, we report that animals can generate a specific form of synaptic activity in a given neuron in the hippocampus. In awake, head-restricted mice, we applied electrical stimulation to the lateral hypothalamus, a reward-associated brain region, when whole-cell patch-clamped CA1 neurons exhibited spontaneous synaptic activity that met preset criteria. Within 15 min, the mice learned to generate frequently the excitatory synaptic input pattern that satisfied the criteria. This reinforcement learning of synaptic activity was not observed for inhibitory input patterns. When a burst unit activity pattern was conditioned in paired and nonpaired paradigms, the frequency of burst-spiking events increased and decreased, respectively. The burst reinforcement occurred in the conditioned neuron but not in other adjacent neurons; however, ripple field oscillations were concomitantly reinforced. Neural conditioning depended on activation of NMDA receptors and dopamine D_1 receptors. Acutely stressed mice and depression model mice that were subjected to forced swimming failed to exhibit the neural conditioning. This learning deficit was rescued by repetitive treatment with fluoxetine, an antidepressant. Therefore, internally motivated animals are capable of routing an ongoing action potential series into a specific neural pathway of the hippocampal network.

Key words: awake mouse; depression; hippocampus; motivation; operant conditioning; synaptic activity

Introduction

Learning is believed to rely on the persistent modification of action potential flow in neuronal networks. Because a neuron has a membrane potential threshold for generating action potentials, it does not fire unless it receives highly synchronized spikes from a presynaptic neuron population. Therefore, learning can be described as a plastic process by which neurons become responsive to specific presynaptic cell assemblies (Hebb, 1949). Cell assembly dynamics have been well documented in coordinated activity of the hippocampus (Harris et al., 2003; Buzsáki, 2010), a brain region involved in certain forms of learning and memory. For example, cell assemblies that appeared during learning are often spontaneously reactivated as synchronous barrages during quiet awake states or slow-wave sleep (Buzsáki et al., 1983; Wilson and McNaughton, 1994; Lee and Wilson, 2002). Therefore, barrage activities of hippocampal neurons serve as an experimental model with which to investigate neural processes underlying learning and memory.

One major form of learning is operant conditioning, in which the frequency of voluntary behavior increases or decreases after reward or punishment (Domjan and Grau, 2003). Half a century ago, Fetz (1969) demonstrated a modified form of the operant conditioning; that is, by the use of neurofeedback training, motor cortical activity in monkeys was operantly reinforced in a given single neuron. More recently, Cerf et al. (2010) reported that humans can voluntarily control the firing rate of a specific neuron in the medial temporal lobe. However, no studies have addressed the synaptic dynamics that mediates the control of a single neuron's firing. Moreover, in these pioneer studies, the activity of the controlled neuron might be correlated with some feature in the real world, including behavior, cognition, attention, and extrinsic rewards such as food or money (Basmajian, 1963; Fetz, 1969; Fetz and Finocchio, 1975; Fetz, 2007; Cerf et al., 2010; Kobayashi et al., 2010; Schafer and Moore, 2011; Sakurai and Takahashi, 2013).

In the present work, we used *in vivo* patch-clamp techniques in the mouse hippocampus and an internal neural process-based paradigm with direct electrical stimulation of the reward system, which did not require an external reward, an explicit cognitive task, or a specific pretraining for the operant conditioning. Using reward stimulation through a real-time neurofeedback system, we attempted to reinforce the event frequencies of the predefined patterns of spontaneous EPSCs (sEPSCs), spontaneous IPSC (sIPSCs), or spontaneous unit activity. In addition, we examined

Received Dec. 19, 2013; revised March 2, 2014; accepted March 6, 2014.

Author contributions: D.I., N. Matsuki, and Y.I. designed research; D.I. and N. Matsumoto performed research; D.I. and T.S. analyzed data; D.I. and Y.I. wrote the paper.

This work was supported by Grants-in-Aid for Science Research on Innovative Areas, "Mesoscopic Neurocircuitry" (Grants 22115003 and 23115101) and "Mental Time" (Grant 25119004) from the Japan Society for the Promotion of Science through the Funding Program for Next Generation World-Leading Researchers (NEXT Program) initiated by the Council for Science and Technology Policy (LS023) and Strategic Research Program for Brain Sciences.

The authors declare no competing financial interests.

Correspondence should be addressed to Yuji Ikegaya, PhD, Laboratory of Chemical Pharmacology, Graduate School of Pharmaceutical Sciences, University of Tokyo, 7-3-1 Hongo, Bunkyo-ku, Tokyo 113-0033, Japan. E-mail: ikegaya@mol.f.u-tokyo.ac.jp.

DOI:10.1523/JNEUROSCI.5298-13.2014

 0270-6474/14/345044-10$15.00/0

how this neural reinforcement learning was modulated by anesthesia or animal's state. As a result, we demonstrated that mice could rapidly learn to receive more reward stimuli by increasing or decreasing the frequency of the predefined activity patterns in a single hippocampal CA1 pyramidal cell. This reinforcement learning did not occur in less motivated animals.

Materials and Methods

Animals. Experiments were performed with the approval of the animal experiment ethics committee at the University of Tokyo (approval number P21-6) and according to the University of Tokyo guidelines for the care and use of laboratory animals. Male C57BL/6J mice (21–27 d old) were housed in cages under standard laboratory conditions (12 h light/dark cycle, *ad libitum* access to food and water). All efforts were made to minimize the animals' suffering and the number of animals used.

Drug. MK801 was applied intraperitoneally (0.1 mg/kg) or locally into the CA1 region. Local application was performed using a pressure injection (16 psi for 20 s) of 300 μM MK801 in artificial CSF (aCSF) consisting of the following (in mM): 127 NaCl, 3.5 KCl, 1.24 KH_2PO_4, 1.2 $MgSO_4$, 2.0 $CaCl_2$, 26 $NaHCO_3$, and 10 D-glucose through glass pipettes (1–3 MΩ). SCH23390 (50 μg/kg) and fluoxetine (20 mg/kg) were applied intraperitoneally.

Habituation. Mice were anesthetized with ketamine (50 mg/kg, i.p.) and xylazine (10 mg/kg, i.p.). Anesthesia was confirmed by the lack of paw withdrawal, whisker movement, and eye blink reflexes. The head skin was then removed and the animal was implanted with a metal head-holding plate. After 2 d of recovery, the head-fixation training on a custom-made stereotaxic fixture was repeated for 1–3 h per day until the implanted animal learned to remain quiet. During and after each session, the animal was rewarded with *ad libitum* access to sucrose-containing water. During the last three sessions, sham experiments were conducted to habituate the animal to experimental conditions and noise. On the last 2–3 d, the animal was kept virtually immobile—quiet but awake—for >2 h.

Electrophysiology. Unanesthetized and head-restrained mice were used unless otherwise specified. After full habituation, the animal was anesthetized with a ketamine/xylazine mixture. A craniotomy (1 × 1 mm^2), centered at 2.2 mm posterior and 2.0 mm lateral to the bregma, was performed and the dura was surgically removed. The exposed cortical surface was covered with 1.7% agar. Throughout the experiments, a heating pad maintained the rectal temperature at 37°C and the surgical region was analgesized with 0.2% lidocaine. After recovery from anesthesia, patch-clamp recordings were obtained using borosilicate glass electrodes (4–7 MΩ). Neurons in the CA1 pyramidal cell layer of the hippocampus or the layer II/III of the primary somatosensory cortex were targeted for patch clamping. In the experiments shown in Figure 3, *D* and *E*, and Figure 5, *I* and *J*, urethane (2.0–2.2 g/kg) was intraperitoneally injected before surgery and electrophysiology was conducted in a manner similar to that for the unanesthetized mice. For voltage-clamped recordings, the intrapipette solution consisted of the following (in mM): 140 Cs-methanesulfonate, 5 HEPES, 10 TEA-Cl, 1 EGTA, 10 2Na-Phosphocreatine, and 1 Mg-ATP, pH 7.2, containing 0.2% biocytin. sEPSCs and sIPSCs were obtained by maintaining the membrane potential at −70 and 0 mV, respectively. For cell-attached recordings, the patch pipettes were filled with aCSF. The signals were amplified and digitized at a sampling rate of 20 kHz using a MultiClamp 700B amplifier and a Digidata 1440A digitizer that were controlled by pCLAMP 10.3 software (Molecular Devices). Data were analyzed offline using custom MATLAB (The MathWorks) routines. Experiments in which the series resistance exceeded 70 MΩ or changed by >15% during the entire recording session were discarded. Hippocampal pyramidal cells were electrophysiologically identified by their characteristic spiking pattern of high-frequency bursts (HFBs; 100–300 Hz, 3–6 spikes) (Kandel and Spencer, 1961; Ranck, 1973) and further confirmed by *post hoc* histological analysis. Data obtained from mice that received conditioning for >20 min under these criteria were used for analysis. Neurons that emitted HFBs at <0.033 Hz (twice per minute) during the preconditioning session were not used. Local field potentials (LFPs) were recorded from CA1 stratum pyramidale using borosilicate glass pipettes (1–2 MΩ) filled with aCSF. The signals were amplified (1000×) and digitized at 20 kHz. LFPs were band-pass filtered between 120 and 250 Hz and the root-mean-square power was calculated by sliding a 10 ms time window at a step interval of 10 ms. Successive time windows during which the ripple power continued to be >3–7× SD were defined as a single ripple epoch. Events shorter than 20 ms were discarded. The coincidence ratio was calculated by dividing the total number of events in which HFBs and ripples occurred simultaneously by the total number of events in which both or either of them occurred.

Real-time feedback delivery of lateral hypothalamus stimulation. After a 5 min session of baseline recording, the distribution of synaptic charges was obtained using a custom-built MATLAB routine. First, synaptic events with amplitudes >7 pA were defined as sEPSCs. This program calculated the difference between the successive local maximums and minimums after local filtering; every event with a peak amplitude larger than 7 pA was regarded as a putative sEPSC (or sIPSC). The onset time, peak time, and offset time of the synaptic event at a threshold of 20% of the peak amplitude above baseline noise were then calculated. Any event with a rise time larger than its decay time was considered a false positive and was discarded from subsequent analyses. Second, the instantaneous amplitude of a synaptic event was integrated from the onset time to the offset time and was defined as a synaptic charge. This procedure was repeated for all detected sEPSCs (or sIPSCs) and the distribution of baseline synaptic charges (i.e., prior distribution) was obtained. Finally, the suprathreshold for detecting $sEPSC_{supra}$s (or $sIPSC_{supra}$s) was set as the top 1% of the distribution. This preset threshold was embedded in a LabVIEW (National Instruments) routine for triggering lateral hypothalamus (LH) stimulation. For cell-attached recordings, HFBs, defined herein as events that included more than two spikes at >100 Hz, were used as a preset criterion for triggering LH stimulation. During operant conditioning, neuronal activities were monitored at a rate of 20 kHz by a custom-made program designed in Linux or a Windows 7 environment. The preset criteria were detected in every 200 and 20 ms segment for voltage-clamped recordings and cell-attached recordings, respectively. When $sEPSC_{supra}$s, $sIPSC_{supra}$s, and HFBs were detected, TTL signals were emitted from a PCI-6024E data acquisition board (National Instruments) to a stimulator and electrical stimulation was immediately delivered to the LH (a reward-related region; AP −1.3 mm; LM −1.0 mm; DV: −5.0 mm) or the ventromedial thalamus (a reward-irrelevant region; AP −1.3 mm; LM −0.8 mm; DV: −3.7 mm). In yoked control experiments, LH stimulation was randomly delivered independently of the preset criteria. Each electrical stimulus consisted of 50 0.1-ms-duration pulses at 100 Hz. The event frequency of the targeted activities ($sEPSC_{supra}$s, $sIPSC_{supra}$s, HFBs, or ripples) was analyzed every 1 min. The frequency was normalized by the baseline mean value during the preconditioning period and their percent changes were expressed as the "%Δ" unit and plotted as a function of time.

Electromyogram. Electromyogram (EMG) electrodes were implanted on the left forelimbs of the mice. EMG signals were amplified, filtered, and digitized at a sampling rate of 20 kHz. All processing was performed *post hoc* using a custom-made MATLAB routine. EMG signals were filtered at 0.01–2 kHz and resampled at 10 kHz. They were then rectified and smoothed using a Gaussian kernel (SD = 25 ms). The power spectrum of 15–300 Hz was calculated every 2 s using the average discrete Fourier transform coefficients.

Whisker movement measurement. Whisker movements were monitored at 1000 Hz using a high-speed CMOS camera. A commercially available image analysis program running in the ImageJ environment was used to measure the whisker angle. Whiskers were considered to have moved when the whisker deflection was 2× SD. The majority of the whisking occurred spontaneously in the absence of overt external events. The whisker angle was integrated over 1 min to assess the whisker movement.

Forced swimming test. Individual mice were forced to swim inside a vertical Plexiglas cylinder (inner φ = 12 cm). The water temperature was 22 ± 1°C, the depth was 15 cm, and the above-water wall height was 8 cm. The mice were kept in the water for 15 min until they spent 60% of their time in immobility. The immobility time was evaluated using a video-based automatic detection system. After mice were removed from the

cylinder, they were dried and used for experiments. In acute-stressed mice, the operant conditioning was started 1–2 h after the forced swimming test for 15 min. In depression-model mice, the operant conditioning was started 1–2 h after the forced swimming test for 5 min on the second day following the same 15 min test on the first day. Saline or fluoxetine (20 mg/kg) was intraperitoneally injected 3 times 1, 19, and 23 h after the forced swimming test on the first day test. The water was changed for each mouse.

Histology. After each experiment, the region of electrical stimulation was histologically confirmed. A direct current (50 μA for 20 s) was administered through the stimulating electrode to mark the position of the electrode tip. Mice were perfused transcardially with 4% paraformaldehyde. The brains were coronally sectioned at a thickness of 100 μm using a vibratome. The lesioned area was located in serial Nissl-stained sessions. Mice in which the intended region was confirmed to be stimulated were used in the data analyses. For biocytin reconstruction, sections were incubated with 0.3% H_2O_2 for 30 min and permeabilized with 0.2% Triton X-100 for 1 h. The sections were processed with ABC reagent (PK-6100; Vector Laboratories) containing 0.2% Triton X-100 at 4°C overnight and developed with 0.0003% H_2O_2, 0.02% diaminobenzidine, and 10 mM $(NH_4)_2Ni(SO_4)_2$. To estimate the spatial diffusion of locally applied MK801, we injected 0.1 mM sulforhodamine 101 (SR101), a fluorescent dye, simultaneously with MK801. After experiments, the animals were perfused transcardially with 0.01 M PBS and then 4% paraformaldehyde. The brains were removed carefully, postfixed overnight at 4°C in 4% paraformaldehyde, and coronally sectioned at a thickness of 100 μm using a DTK-1500 vibratome (Dosaka). The sections were incubated with 0.5 μg/ml Hoechst 33342 for 5 min. The dye-injected area was visualized using a macrozoom fluorescence microscope (MVX10 MacroView; Olympus).

Results

Reinforcement of synaptic activity

We used a closed-loop system in which ongoing activity of a patch-clamped neuron in a mouse was analyzed online at an update rate of 20 kHz and applied feedback stimulation to the brain of the same animal (Fig. 1*A*). In an awake, head-fixed mouse, a single dorsal hippocampal CA1 pyramidal neuron was voltage clamped at −70 mV to monitor sEPSCs (Fig. 1*B*). A tungsten-stimulating electrode was implanted in the ipsilateral LH, one of the reward-related regions of the brain (Margules and Olds, 1962). First, we collected sEPSCs for 5 min and obtained the "prior" distribution of the area above the curves of individual sEPSC events (sEPSC charges). We then defined the preset threshold as the top 1% of sEPSC charges in this prior distribution and started operant conditioning (Fig. 1*C*).

During the conditioning session, we continued to monitor sEPSCs for at least 20 min (Fig. 2). When a sEPSC larger than the preset threshold ($sEPSC_{supra}$) was recorded, an electrical rewarding stimulus (50 pulses at 100 Hz; pulse width of 0.1 ms; pulse amplitude of 30–40 μA) was immediately delivered to the LH (Fig. 2*A*) in <50 ms delay. The mean frequency of $sEPSC_{supra}$s was 0.19 ± 0.03 Hz during the preconditioning baseline period (mean ± SEM of 19 cells from 19 mice; Fig. 3*A*). The $sEPSC_{supra}$ frequency started to increase ~5 min after the onset of the conditioning and reached a steady state at an increased level of 126.6 ± 45.2% (mean ± SEM of 9 cells, $p = 0.0091$, $t_8 = 3.41$, paired t test; Fig. 2*B*, closed circles, Fig. 3*C*, left). This increment was observed regardless of the initial $sEPSC_{supra}$ frequency (Fig. 2*C*) and persisted for at least 10 min after termination of the LH stimulation (Fig. 2*B*). In a single whole-cell recording, we routinely measured the membrane properties during the preconditioning and postconditioning sessions and did not find that the neuron exhibited a change in the intrinsic excitability (data not shown), suggesting that the increase in $sEPSC_{supra}$s was unlikely to be a result of the overall trend of neuronal excitation. Consistent with this idea, the overall mean frequency of subthreshold sEPSCs ($sEPSC_{sub}$s) was not changed by the conditioning (Fig. 3*C*, right), although the top 10% of $sEPSC_{sub}$s were reinforced (Fig. 2*D*). The conditioning did not alter the mean charges of $sEPSC_{supra}$s ($p = 0.38$, $t_8 = 0.92$, paired t test; Fig. 2*B*, open circles). In three trained mice, we also monitored the electromyogram power of their forelimbs and the movement of their whiskers, but we did not observe apparent changes in the body motion level during the conditioning (Fig. 2*E*). LH stimulation did not reinforce the $sEPSC_{supra}$ frequency in urethane-anesthetized mice ($p = 0.99$, $t_4 = 0.013$, paired t test, $n = 5$ cells; Fig. 3*D*,*E*).

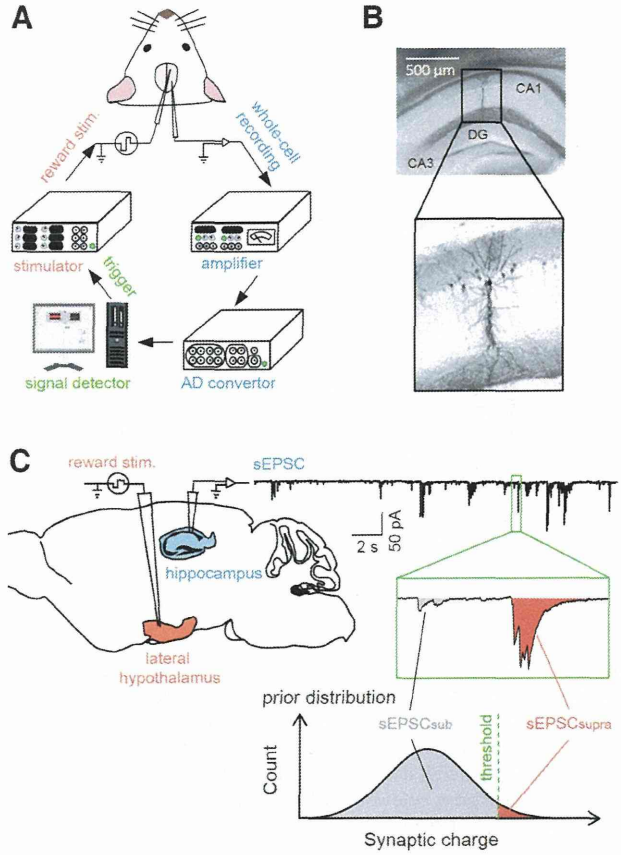

Figure 1. Experimental paradigm for a closed-loop neurofeedback system. ***A***, Whole-cell recordings of sEPSCs were obtained from CA1 pyramidal cells in awake mice and were digitized at 20 kHz after amplification. The largest 1% of sEPSCs detected were used to trigger electrical reward stimulation. ***B***, Representative biocytin reconstruction of a whole-cell-recorded CA1 neuron. ***C***, The prior distribution of sEPSC charges was obtained during a baseline period of 5 min and the top 1% was defined as a preset threshold between $sEPSC_{supra}$s and $sEPSC_{sub}$s. Reward stimuli were applied to the LH immediately after the occurrence of individual $sEPSC_{supra}$s.

To examine the involvement of NMDA receptors, which are known to be involved in the induction of synaptic plasticity in hippocampal excitatory transmission, we treated mice with intraperitoneal administration of 0.1 mg/kg MK801, an NMDA receptor antagonist, 15–30 min before conditioning. MK801 prevented neural operant conditioning ($p = 0.53$, $t_4 = 0.69$, paired t test, $n = 5$ cells; $p = 0.021$, Bonferonni's/Dunn's test vs reinforcement; Fig. 3*B*,*C*, left), whereas MK801 per se did not alter the $sEPSC_{supra}$ frequency during the preconditioning period ($p = 0.92$, $t_{22} = 0.10$, Student's t test; Fig. 3*A*).

As a control, we used a random trigger generator and arbitrarily applied LH stimulation regardless of the $sEPSC_{supra}$ timing. In this yoked conditioning, the timing of LH stimulation was